Journal of Solid State Chemistry 184 (2011) 1105–1111

Contents lists available at ScienceDirect

Journal of Solid State Chemistry

journal homepage: www.elsevier.com/locate/jssc

Direct comparison between two γ-alumina structural models by DFT calculations

Ary R. Ferreira [a], Mateus J.F. Martins [a], Elena Konstantinova [b], Rodrigo B. Capaz [c], Wladmir F. Souza [d], Sandra Shirley X. Chiaro [d], Alexandre A. Leitão [a,*]

[a] Departamento de Química, Universidade Federal de Juiz de Fora, Juiz de Fora, MG 36036-330, Brazil
[b] Departamento de Ciências da Natureza, IFSudeste MG, Juiz de Fora, MG 36080-001, Brazil
[c] Instituto de Física, Universidade Federal do Rio de Janeiro, Caixa Postal 68528, Rio de Janeiro, RJ 21941-972, Brazil
[d] PETROBRAS-CENPES, Ilha do Fundão, Rio de Janeiro, RJ 21941-915, Brazil

ARTICLE INFO

Article history:
Received 1 November 2010
Received in revised form
24 February 2011
Accepted 6 March 2011
Available online 15 March 2011

Keywords:
γ-alumina
Ab initio
DFT
Electronic structure
Structural model

ABSTRACT

We selected two important γ-alumina models proposed in literature, a *spinel-like* one and a *nonspinel* one, to perform a theoretical comparison. Using *ab initio* calculations, the models were compared regarding their thermodynamic stability, lattice vibrational modes, and bulk electronic properties. The *spinel-like* model is thermodynamically more stable by 4.55 kcal/mol per formula unit on average from 0 to 1000 K. The main difference between the models is in their simulated infrared spectra, with the *spinel-like* model showing the best agreement with experimental data. Analysis of the electronic density of states and charge transfer between atoms reveal the similarity on the electronic structure of the two models, despite some minor differences.

1. Introduction

Low temperature alumina (Al_2O_3) phases are very important in catalysis due to their high specific surface areas, the mechanical and thermal resistance, and the large number of defects in their crystalline structure [1]. The calcination of boehmite (γ-AlO(OH)), bayerite (α-$Al(OH)_3$) and gibbsite (γ-$Al(OH)_3$) results in the most stable product α-Al_2O_3 above 1273 K. Furthermore, at intermediate temperatures, different phases of aluminium oxide can be observed for each kind of precursor [2]. Among these intermediate phases called transition aluminas (η, γ, χ, δ, κ and θ), γ-alumina (γ-Al_2O_3) is regarded as an extremely important material in many industrial processes acting as an adsorbent, a catalyst and/or catalyst support [3]. In petroleum and petrochemical industries γ-alumina is used as catalyst support for transition-metal sulfides Co(Ni)MoS in hydrotreatment catalysts and metallic alloys in reforming catalysts [4]. Due to its low crystallinity and the consequent difficulty of characterization, the debate on the structure of γ-alumina remains open and a series of theoretical and experimental works [1,5–11] concerning this subject have been published along the decades. Another complicating factor related to the structural characterization issue is the synthetic route, in which the thermal treatment required to obtain γ-alumina varies with each type of precursor [2]. The correct temperature in which the γ phase is obtained with a high degree of purity cannot be determined, hampering the structural characterization by X-ray diffraction (XRD) experiments. The main discrepancies between various published results concern the distribution of vacancies among octahedral and tetrahedral sites, and the occupation of only spinel sites or nonspinel sites. This issue was well summarized by Paglia et al. [12].

Some experimental works [9–12] about the γ-alumina crystallographic structure reported a *spinel-like* structure with a cubic unit cell and the $Fd\bar{3}m$ space group. On the theoretical side, the classical way to propose the γ-alumina structure is to start from an original spinel cubic unit cell [13], replace each Mg atom by an Al atom, resulting in a cell with 64 atoms. Then, the primitive unit cell which contains 14 atoms is obtained and three of such cells are stacked to form a γ-alumina cell with 42 atoms. Finally, two Al atoms, selected by an energetic criterion, are replaced by vacancies resulting in a cell with 8 Al_2O_3 units, called *defect spinel* or *spinel-like* structure.

Boehmite is the topotactic precursor of γ-alumina and in that case the precursor bequeaths the bulk properties to the final product [8]. Based on this idea, Krokidis et al. [7] proposed a skeleton for γ-alumina. The approach consists of a theoretical

* Corresponding author.
E-mail address: alexandre.leitao@ufjf.edu.br (A.A. Leitão).

0022-4596/$ - see front matter © 2011 Elsevier Inc. All rights reserved.
doi:10.1016/j.jssc.2011.03.016

study of the elementary steps of boehmite dehydration process using molecular dynamics simulation and first principles calculations within the density functional theory (DFT) framework [14,15]. In [7], it was simulated the loss of 100% of water by boehmite layered structure, resulting in its collapse summarized by

$$2n\mathrm{AlOOH} \rightarrow n(\square \mathrm{Al_2O_3}) + n\mathrm{H_2O} \quad (1)$$

As a following step, it was simulated the aluminum migration towards tetrahedral and/or octahedral sites allowed by the vacancy ($\square$) distribution. The main result was a structure of γ-alumina with 25% of tetrahedral sites and a good agreement between the simulated XRD patterns and experimental ones. This result of tetrahedral sites distribution was also obtained by ^{27}Al Nuclear Magnetic Resonance (NMR) experiments [16].

Another important theoretical reference is the work of Gutiérrez et al. [17], published in the same year as [7], in which a crystallographic structure was proposed for γ-Al_2O_3 with only octahedral vacancies. The calculated electronic structure was compared with experimental X-ray Photoelectron Spectroscopy (XPS) data. Following this work, Pinto et al. [18] proposed a γ-alumina structure using DFT in the same way as Gutiérrez et al. [17], reporting a primitive cell with C2/m space group and both vacancies on octahedral sites, complementing their work with studies of (111), (001), (110) and (150) surfaces. Using interatomic potentials and first-principles calculations, Paglia et al. [19] verified that, in average, over 40% of the cations must occupy *nonspinel* positions to achieve an accurate structural model while the optimization of *spinel-like* structural models led to less favorable energies. More recently, a debate in literature [20–23] about the inability of a *nonspinel* model to describe the γ-alumina bulk and other publications stating just the opposite [12,19,24], leaves some doubts about which model to choose when the goal is to simulate surfaces.

In the last decade, several theoretical works describing the electronic properties of bulk and physical–chemical processes over γ-alumina surfaces were published using both *spinel-like* [18,25–29] and *nonspinel* [4,30–32] models. From this point of view, a bulk model well-validated by experimental results is a necessary condition for the success of slab models to be used in surface calculations. Furthermore, a unitary cell with no fractional occupations and all atomic coordinates (or the asymmetric unit together with the space group) explicitly disclosed in literature can greatly simplify the creation of surface models. Good examples of those types of publications are the work of Digne et al. [4], who published a detailed study of the bulk electronic structure properties and the (100), (110), and (111) surfaces, and the work of Menéndez-Proupin and Gutiérrez [33], who studied the γ-alumina bulk electronic structure with DFT and made a comparison of simulated XRD patterns of seven different structural models.

It is well-known that all relevant processes related to catalysis occur over the surfaces of solids and many researchers adopt one of the different γ-alumina structures to propose slab models and simulate physical–chemical processes over their surfaces. Bermudez [26] used the *spinel-like* model of Pinto et al. [18] to propose Al_8O_{12} and $Al_{20}O_{30}$ cluster models of the (111) surface and simulated using DFT the adsorption of the chemical warfare agent simulator dimethyl methylphosphonate (DMMP) and the corresponding real agent Sarin. Pan et al. [34] investigated the adsorption and protonation of CO_2 on the (110) and (100) surfaces using DFT and periodic boundary conditions with the *nonspinel* model proposed by Krokidis et al. [7]. Bermudez [27] used again the Pinto et al. [18] model to study the adsorption of DMMP, Sarin, and O-ethyl S-[2-(diisopropylamino)ethyl] methylphosphonothioate (VX) over the (111) surface taking into account environmental effects, namely, surface hydroxylation and photoexcitation with time-dependent DFT (TDFT). Adopting the Krokidis et al. [7] model, Chizallet et al. [31] studied the geometry, stability and vibrational properties of OH groups on (110), (100), and (111) surfaces by DFT calculations. With the same model, Feng et al. [32] studied the adsorption of isopropanol on the clean and hydrated (100) and (110) surfaces within DFT. The *spinel-like* model of Pinto et al. [18] was also used by Chen et al. [28] within the DFT to study the deposition of Ir atoms on (001) surface. As an example of this type of study using a different model (but also *spinel-like* one), Ouyang et al. [29] applied the *spinel-like* cubic structure with the $Fd\bar{3}m$ space group to investigate the atomic and electronic structure of the (001) surface using DFT.

In this work we performed a direct comparison between *spinel-like* and *nonspinel* models of γ-alumina with respect to their thermodynamic stability in the temperature range from 0 to 1000 K, lattice vibrational modes, and bulk electronic properties using *ab initio* calculations. Recent works [35,36] confirm that the electron density and calculated properties are very sensitive to the accurate relaxation of the structures. So after the relaxation of the choosed structures, the thermodynamic and vibrational analysis pointed to the *spinel-like* model as the most realistic to understand the γ-alumina bulk structure, even though the electronic distribution around oxygen and aluminum atoms are very similar.

2. The Al_2O_3 models

2.1. The γ phase spinel-like model

The adopted *spinel-like* γ-alumina model was proposed by Menéndez-Proupin and Gutiérrez [33]. The cell contains 8 Al_2O_3 units where 37.5% of the cations are Al_{tet} and 62% Al_{oct}, and of 24 O atoms, 12 are $O_{4\text{-}fold}$ and 12 are $O_{3\text{-}fold}$ [25]. The crystal system is triclinic but approximately hexagonal, with lattice parameters presented in Table 1. This model and the one proposed by Pinto et al. [18] are almost identical, and the direction of [001] vector of those models coincides with the [111] direction in the cubic spinel structure [18]. Therefore, to obtain a slab model of the (111) γ-alumina surface with that cell it is sufficient to create a supercell with vacuum in the ***c*** direction.

2.2. The γ phase nonspinel model

The *nonspinel* γ-alumina model was proposed by Krokidis et al. [7] and explicitly provided by Digne et al. [4]. Such a crystallographic cell also contains 8 Al_2O_3 units, the sublattice of

Table 1
Structural parameters for the two γ phase models and for the α phase model.

	Original [33]	Relaxed
Spinel-like		
Vectors (Å)	**a**=5.606, **b**=5.570, **c**=13.482	**a**=5.647, **b**=5.611, **c**=13.591
Angles (deg)	$\alpha=89.4$, $\beta=90.0$, $\gamma=120.2$	$\alpha=89.5$, $\beta=90.0$, $\gamma=120.2$
	Original [7]	Relaxed
Nonspinel		
Vectors (Å)	**a**=5.587, **b**=8.413, **c**=8.068	**a**=5.543, **b**=8.352, **c**=8.026
Angles (deg)	$\alpha=\gamma=90.0$, $\beta=90.6$	$\alpha=\gamma=90.0$, $\beta=90.5$
	Original [37]	Relaxed
α-Al_2O_3		
Vectors (Å)	**a**=**b**=4.754, **c**=12.990	**a**=**b**=4.786, **c**=13.065
Angles (deg)	$\alpha=\beta=90.0$, $\gamma=120.0$	$\alpha=\beta=90.0$, $\gamma=120.0$

O^{2-} anions is FCC, 25% of Al^{3+} cations are Al_{tet} and 75% are Al_{oct}. The crystal system is monoclinic, but very close to an orthorhombic one with lattice parameters presented in Table 1 and $P2_1/m$ space group. The morphology of this bulk model is quite interesting from a practical point of view, because its lattice system is almost tetragonal and due to the structural and morphological relations between boehmite and γ-alumina surfaces [4], the slab models for (100) and (110) surfaces are immediately obtained by creating supercells with vacuum in the ***c*** and ***b*** directions, respectively.

2.3. The α phase model

The structural model for α-alumina used as a reference in this work was published by Ishizawa et al. [37] in a XRD study. The structure was reported as a corundum-type, with an hexagonal crystal system and $R\bar{3}c$ space group with lattice parameters presented in Table 1. The crystallographic cell contains 6 Al_2O_3 units and will be used in this work as a reference in the thermodynamic and the electronic structure analyses of the two γ-alumina models studied in this work. There are more recent works on the α-alumina structure [38,39], however, the differences between the lattice parameters from these works and the lattice parameters from Ishizawa et al. [37] (up to 0.003 Å in the lattice vectors) are smaller than the differences related to the structure relaxation showed in Table 1 (up to 0.07 Å in the lattice vectors). The relaxed lattice parameters are in satisfactory agreement with the experimental values with discrepancies of 0.7% and 0.6% for the **a** and **c** parameters, respectively.

3. Theoretical methodology

All the *ab initio* calculations were performed using the PWSCF [40] code which implements the DFT framework with periodic boundary conditions. We also used a plane waves basis set to expand the one-electron wavefunctions of Kohn–Sham equations [15], whose Hamiltonian exchange correlation potential was described by the PW91 [41] Generalized Gradient Approximation (GGA). The core electrons were treated with Vanderbilt [42] ultrasoft pseudopotentials and the k-points sampling for the integration in the Brillouin zone (BZ) were determined by the Monkhorst–Pack [43] procedure. Convergence tests for the plane wave ($\mathbf{k}+\mathbf{G}$) cut-off were made for all bulk models and defined in terms of a kinetic energy of 60 Ry with a cut-off for charge density and potential of 480 Ry. The k-points sampling convergence tests were also performed and the $2\times2\times1$ Monkhorst–Pack sampling was chosen for the three models. The atomic structure of cells were fully optimized (atomic positions and vectors) with a convergence threshold on total energy of 1×10^{-4} Ry, without significant changes compared to the original structures. After the relaxation, all post processing calculations were performed using a $4\times4\times4$ Monkhorst–Pack k-points sampling and a convergence threshold for self-consistency of 1×10^{-10} Ry.

The vibrational modes were obtained from phonon calculations, based on a harmonic approximation, of each structure at Γ q-point. The PHonon code [40] implements the density-functional perturbation theory (DFPT) [44–46] for the calculation of second- and third-order derivatives of the energy with respect to atomic displacements and to electric fields. The vibrational modes were obtained from phonon calculations of each structure with only Γ q-point, preceded by a single point electronic structure calculation of optimized structures with a kinetic energy cut-off of 60 Ry, a cut-off for charge density and potential of 480 Ry and a convergence threshold for self-consistency of 1×10^{-10} Ry. The threshold for convergence in phonon calculations was set to 1×10^{-14}.

Thermodynamic data were obtained from the partition function [47] with only *vibrational* contributions. The total entropy, S, is given by the vibrational contribution, S_v,

$$S=S_v=N_Ak_b\sum_k\left[\frac{\frac{\Theta_{v,k}}{T}}{\exp\left(\frac{\Theta_{v,k}}{T}\right)-1}-\ln\left(1-\exp\left(-\frac{\Theta_{v,k}}{T}\right)\right)\right].$$

The total internal energy, U, is

$$U=E_{DFT}+U_{ZPE}+U_v=E_{DFT}+U_{ZPE}+N_Ak_b\sum_k\left[\frac{\Theta_{v,k}}{\exp\left(\frac{\Theta_{v,k}}{T}\right)-1}\right],$$

where N_A, k_b, and $\hbar$ are the Avogadro, Boltzmann and reduced Planck constants, respectively. $\Theta_{v,k}$ are the vibrational temperatures,

$$\Theta_{v,k}=\frac{\hbar\omega_k}{k_b},$$

and the summations are over all vibrational modes k. E_{DFT} is the total electronic energy obtained from the *ab initio* calculations, and the zero point energy is given by

$$U_{ZPE}=\frac{N_Ak_b}{2}\sum_k\Theta_{v,k}. \quad (2)$$

At ambient pressure, the $p\Delta V$ term in the variation of enthalpy (ΔH) gives very small contributions per formula unit for both phases. Thus, we can consider

$$\Delta H\approx\Delta U.$$

As a result of this approximation, the variation of Gibbs (ΔG) and Helmholtz (ΔA) energies are given by

$$\Delta G\approx\Delta A=\Delta U-T\Delta S.$$

4. Results and discussion

4.1. Vibrational and thermodynamic analysis

For the *spinel-like* bulk model, 117 phonon wavenumbers between 97.4 and 887.4 cm^{-1} with their respective absorption infrared intensities, were obtained from the calculations. For each vibrational mode and its respective calculated intensity a Lorentzian distribution curve with a full width at half maximum of 20 cm^{-1} was plotted. From the convolution of all 117 distribution curves, a simulated vibrational infrared (IR) spectrum was obtained, from which it is possible to highlight four bands with maxima at 390.7 cm^{-1} (medium), 483.8 cm^{-1} (strong), 627.7 cm^{-1} (medium), 780.0 cm^{-1} (medium), plus an additional shoulder-type maximum at 725.0 cm^{-1} (weak). The same mathematical treatment was performed with the 117 phonon frequencies between 149.1 and 860.8 cm^{-1} calculated for the *nonspinel* bulk model. From this simulated spectrum, it is possible to check five bands with maxima at 439.8 cm^{-1} (strong), 534.0 cm^{-1} (medium), 570.9 cm^{-1} (medium), 644.6 cm^{-1} (medium-weak), 742.9 cm^{-1} (weak), plus four shoulder-type maxima at 321.0 cm^{-1} (weak), 378.4 cm^{-1} (medium), 681.5 cm^{-1} (medium-weak), 837.1 cm^{-1} (weak). The simulated IR spectra of the two models are presented in Fig. 1. An experimental study was conducted by Saniger [48], in which the IR spectrum of the γ-alumina was interpreted based on the band assignment of the IR spectra of the spinels. The author made a deconvolution

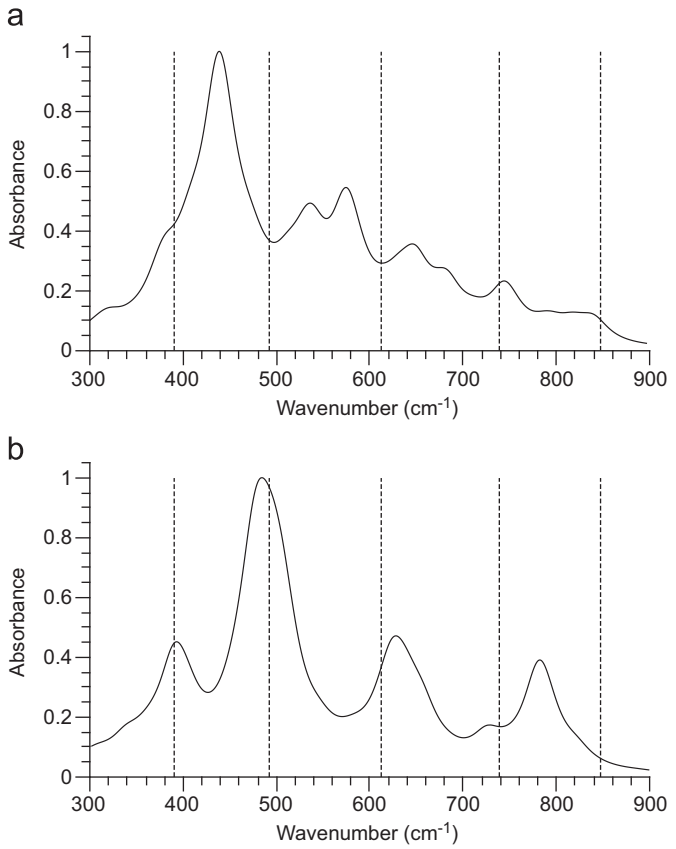

Fig. 1. Simulated infrared spectra for (a) the *nonspinel* and (b) the *spinel-like* models. The dashed black lines represent the experimental frequencies of Saniger [48].

analysis of the broad unresolved experimental band between 300 and 1100 cm^{-1} and, by examining the deconvoluted bands, six bands centered at 390.7 cm^{-1} (medium), 491.6 cm^{-1} (medium), 613.0 cm^{-1} (strong), 738.6 cm^{-1} (medium-strong), 846.9 cm^{-1} (medium-strong), and 931.4 cm^{-1} (medium-strong) were detected. Before any attempt to assign the 117 phonon frequencies calculated for both structural models, it is possible to verify that the simulated spectrum for the *spinel-like* model is more similar to the experimental deconvoluted one than the simulated spectrum for the *nonspinel* model. In a recent publication, Loyola et al. [49] used classical force fields to simulate the IR spectra for the same two models adopted in this work, limiting the discussion on the differences between theoretical spectra of the different structural models. Their simulated IR spectrum for the *spinel-like* model is qualitatively similar to the one presented in Fig. 1(b), whilst for the *nonspinel* model this agreement does not exist.

In the last cited experimental work [48], the assignment of the band at 390.7 cm^{-1} was based on the existence of H^+ cations in tetrahedral sites of γ-alumina, what has been discarded in a later study [5]. The following three bands were assigned to complex AlO_4 and AlO_6 interactive vibrations and alternatively to the stretching (symmetric or asymmetric) of condensed AlO_6 groups or isolated AlO_4 groups. The two left medium-strong bands could not be assigned to structural coordinated groups of γ-alumina and were considered as complex vibrations of the unit cell as a whole. The vertical dashed black lines presented in Fig. 1 represent the experimental frequencies except the one at 931.4 cm^{-1}, which can be assigned to adsorbed species over the surface. The assignment of each one of the four simulated bands with better accordance to the experimental ones in the *spinel-like* spectrum, Fig. 1(b), was done considering only the calculated vibrational modes with higher intensities, whose distributions contribute to the band in question. The first with maxima at 390.7 cm^{-1} is assigned to asymmetric stretching of two condensed AlO_4 groups. The next one at 483.8 cm^{-1}, is mainly related with asymmetric stretching of two condensed AlO_6 groups in the crystallographic cell. The last maximum at 627.7 cm^{-1} can only be attributed to complex AlO_4, and AlO_6, interactive vibration. Finally the shoulder-type maximum at 725.0 cm^{-1} is assigned to two AlO_4 groups interactive vibration. Thus, besides the theoretical spectrum of the *spinel-like* model present a good agreement with the profile of the experimental spectrum, the assignments of the simulated bands are also in agreement with those made in the experiment of Saniger [48].

We found the total electronic energy (without vibrational corrections) of the *spinel-like* model to be 4.09 kcal/mol (0.18 eV) per Al_2O_3 units more negative than the energy of the *nonspinel* model. The zero point energies, Eq. (2), were computed based on formalism presented in Section 3 for *spinel-like* and *nonspinel* models, the calculated values are 10.15 and 10.27 kcal/mol per formula unit, respectively. The difference in these zero point energy values are related to the unconformity between the simulated IR spectra from Fig. 1. With respect to the standard conditions for temperature and pressure, every system seeks to achieve a minimum of the free energy. Fig. 2 shows a comparison between the Gibbs free energies and the enthalpies of the inverse phase transition of Eq. (3), for both models in the temperature range from 0 to 1000 K:

$$\alpha Al_2O_3 \rightarrow \gamma Al_2O_3 \quad (3)$$

The average difference in the Gibbs free energy (Fig. 2(a)) between the two models over that temperature range is 4.55 kcal/mol.

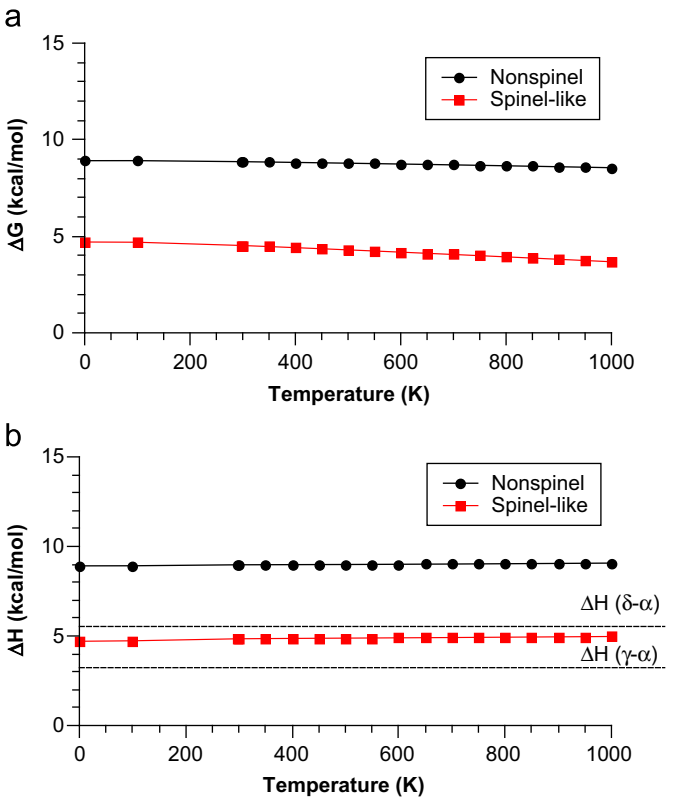

Fig. 2. Thermodynamic comparison between the phase transition proposed by Eq. (3) of two γ-alumina models and α-alumina (Corundum). Gibbs free energies (a) and enthalpies (b) are given in kcal/mol per formula unit, over a temperature range of 0–1000 K. The region between the two black horizontal dashed lines correspond to measured enthalpies for the $\alpha \rightarrow \gamma$ and $\alpha \rightarrow \delta$ transitions, named $\Delta H(\gamma - \alpha)$ and $\Delta H(\delta - \alpha)$, respectively.

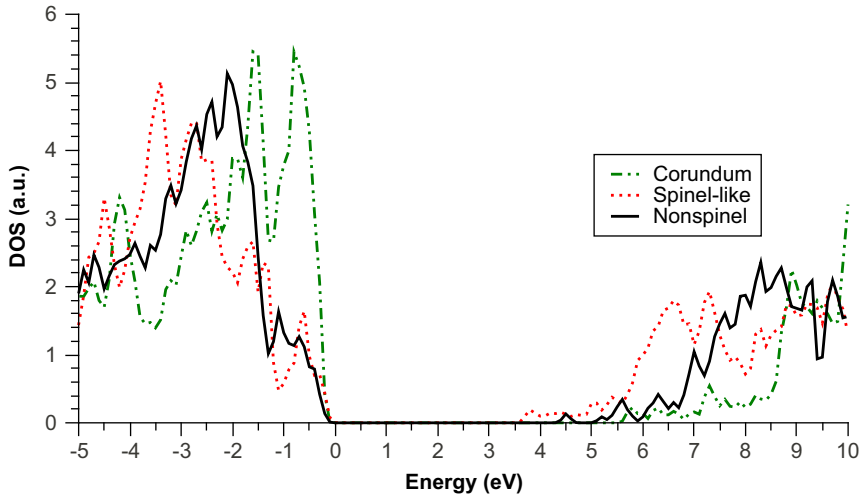

Fig. 3. Calculated DOS for *nonspinel*, *spinel-like* γ-alumina models and α-alumina (Corundum). The densities were divided by the number of Al_2O_3 units in each cell.

There are some theoretical works [5,17,18] from literature, in which the analysis of the energetically preferred vacancy configurations for spinel based structural γ-alumina models were done. In these works, the criterion to choose the best structural models was simply the electronic energy (with no mention to zero-point or thermal corrections) for the transformation given by the Eq. (3), and the average difference between the most energetically favorable ones was 3.23 kcal/mol. It can be noted, by inspection of Fig. 2(a), that the Gibbs free energy for the formation of γ-alumina from α-alumina, as expected for materials with strong covalent bonds, is not sensitive to the temperature. Since the Gibbs energy is a state function, the formation energy of *nonspinel* γ-alumina from *spinel-like* is almost constant and can be approximated by 4.55 kcal/mol. A comparison between the charts (a) and (b) in Fig. 2, shows that the main contributions to the ΔG values are given by the ΔH (or ΔU) terms and the $-T\Delta S$ terms contributions are slightly more significant for the *spinel-like* model. Thus, the calculated ΔH variation with the temperature can be used to compare both γ-alumina models with experimental thermochemical data. A piece of information presented in Fig. 2(b) is related to the "experimental transformation enthalpies" region between 3.23 and 5.53 kcal/mol, marked with two dashed black lines. This region in the range of measured enthalpies of transformation for the $\alpha \rightarrow \gamma$ and $\alpha \rightarrow \delta$ transitions, mentioned by other related studies [5,18], referring to thermochemical data obtained in some experimental works [50–52] and used as a basis of comparison between electronic energy of different structures calculated at $T=0$. The chart of Fig. 2(b) shows that the *spinel-like* model falls within the experimental region over the entire temperature range, whilst the *nonspinel* one falls off over the entire range. This observation indicates that the *spinel-like* model is more favorable from the thermodynamic point of view.

4.2. Electronic structure

A comparison of the simulated density of states (DOS) of the two γ phase models with the α phase one [37], used as reference in the thermodynamic analysis, is presented in Fig. 3. In α-alumina, all cationic sites are octahedral and there is a considerable difference between the DOS of the different alumina phases. The region between -2 and 9 eV shows that the O^{2-} and Al^{3+} ions of α phase are more basic and less acidic, respectively, than the γ phase. Besides, an analysis of the Fig. 3 reveals that the simulated DOS of the two γ phase models are quite similar to each other, if compared with the DOS of the α phase.

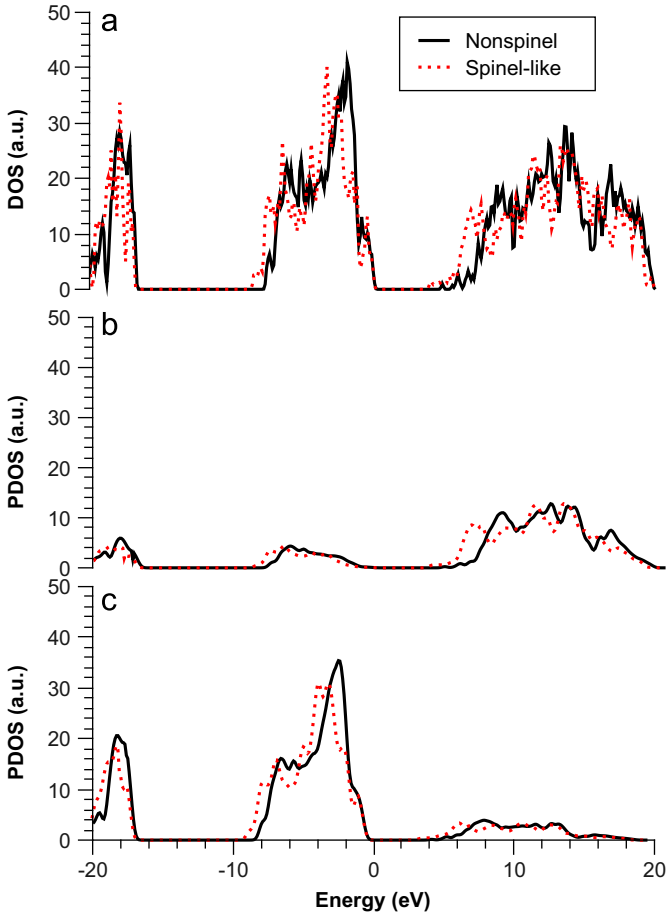

Fig. 4. Calculated DOS and PDOS for *spinel-like* and *nonspinel* models. (a) Total DOS, (b) PDOS of Al atoms, and (c) PDOS of O atoms.

The calculated electronic band structure of both models exhibits similar profiles with respect to the valence and the conduction bands, as it can be seen in the DOS chart of Fig. 4(a). Two regions are evident in the valence band of the *spinel-like* model, the first one approximately from -20.29 to -15.95 eV and the second one from -7.27 eV to the Fermi level, separated by a gap of approximately 8.68 eV. It is well-known that DFT underestimates the gap between the valence and the conduction bands which was about

4.34 eV, in contrast to the experimental value of 8.5 eV [53]. The same is observed in the analysis of electronic band structure of *nonspinel* model, in which the two regions in the valence band are located from −19.83 to −16.11 eV and from −6.19 eV to the Fermi level, separated by a gap of about 9.92 eV. The gap between the valence and the conduction bands was approximately 4.96 eV. Moreover, an analysis of Fig. 4(b) and (c) reveals that there is a low contribution from Al PDOS in the valence band and a low contribution from O PDOS in the conduction band, what reveals a weak covalence in this compound.

The DOS of the two models presents a considerable qualitative and quantitative agreement, except for the region between 4 and 9 eV, where the DOS is almost exclusively of the *spinel-like* model. To determine which are the atomic species responsible for the DOS in this energy region, it is useful to analyze the partial density of states (PDOS) of Al^{3+} cations and O^{2-} anions. The PDOS of O atoms, Fig. 4(c), are very similar for both models, while the PDOS of Al atoms, Fig. 4(b), shows that the unoccupied electronic states with lower energies of these atoms are responsible for the discrepancy in the region between 4 and 10 eV. That is in accordance with all discussion presented above in this document, about the historical difficulty to define a Al^{3+} sublattice that can be corroborated by experimental data, while the O^{2-} sublattice is more well defined.

As discussed in this work, there are Al_{tet} and Al_{oct} in both models among the Al^{3+} cations. So the total PDOS of Al atoms can be decomposed by their coordination numbers, as shown in Fig. 5. In Fig. 5(a) we show the PDOS of all Al atoms from *nonspinel* model and the contribution of each kind of cation, revealing that in this model the contributions of Al_{tet} and Al_{oct} are the same between 4 and 9 eV. However, the same analysis of Fig. 5(b) points that in the *spinel-like* bulk model, only Al_{tet} contributes to DOS in the same energy range. The distinct Al_{oct}/Al_{tet} ratios in the two models must be regarded when comparing the density in Fig. 6, which shows that Al_{tet} of the *spinel-like* bulk model presents unoccupied states with energies about 2 eV smaller than Al_{tet} of the *nonspinel* one.

From an orbital-resolved PDOS analysis (ORPDOS), Fig. 7, it was possible justify that difference pointed above. The Al_{tet} in both models should be sp^3 hybridized and it was perfectly described by the simulated electronic structure of the *spinel-like* model in Fig. 7(b). On the other hand, the ORPDOS analysis for the *nonspinel*,

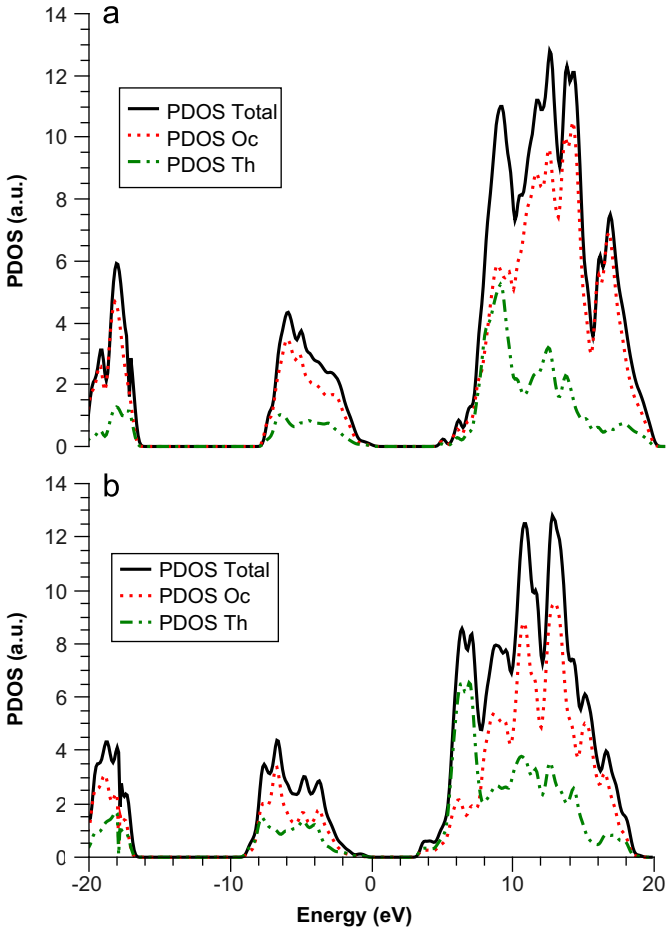

Fig. 5. Calculated PDOS of Al atoms. (a) Contribution of Al_{oct} and Al_{tet} for the Al total PDOS on *nonspinel* and (b) on *spinel-like* models.

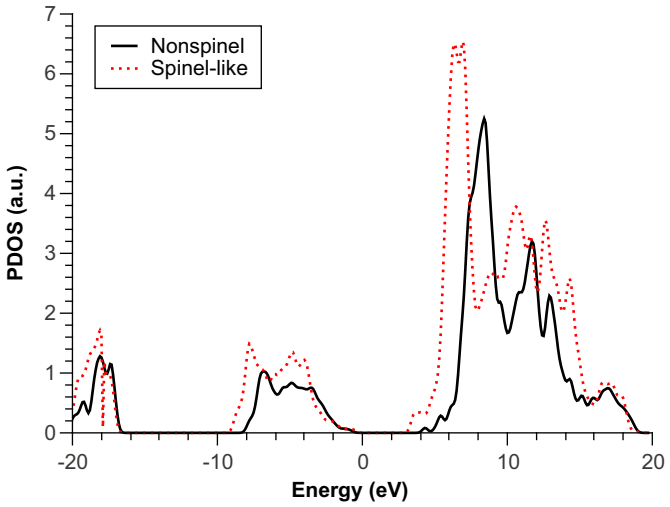

Fig. 6. A comparison between Al_{tet} PDOS of the two models.

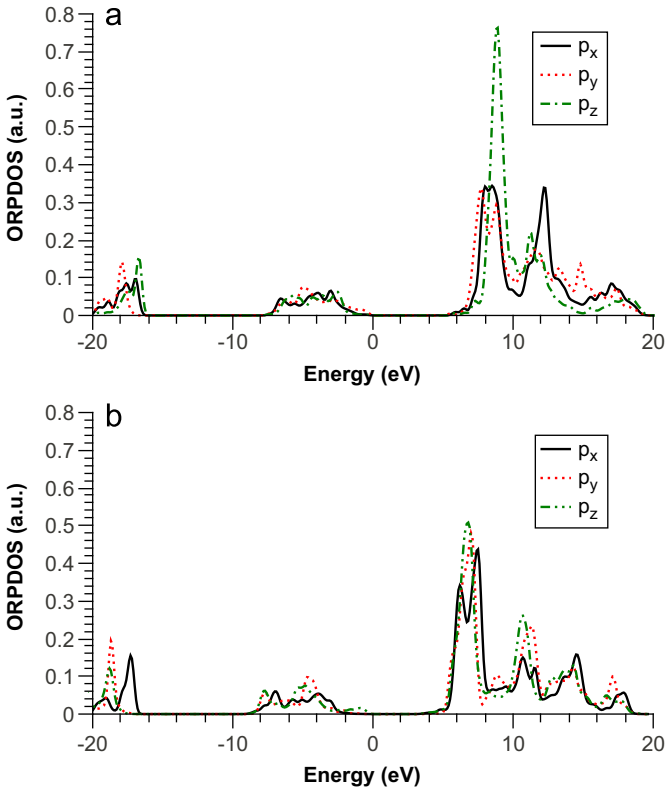

Fig. 7. A comparison between one Al_{tet} ORPDOS in the (a) *nonspinel* and in the (b) *spinel-like* models.

Fig. 7(a), revealed a break in the degeneracy in these states with an considerable increase in the density of the p_z states at 8.5 eV, just the energy level of the major peak checked in the PDOS of Al_{tet} atoms in the *nonspinel* model, Fig. 6. These features in the electronic structure of Al_{tet} atoms in both models are closely related to the different degrees of tetrahedral distortion in these sites. In the *spinel-like* model, they are almost regular with the four O–Al–O (107.892°, 110.045°, 110.018°, 107.910°) angles close to the ideal value, 109.47°, whilst in the *nonspinel* model the tetrahedron is more distorted (105.274°, 105.821°, 111.145°, 111.788°), explaining the breaking of the degeneracy of the sp^3 hybrid states. Moreover, even being a ground state method, the DFT could describe the expected electronic states for the unoccupied bands given the geometric distortions of the systems. Recalling that the two compared systems have exactly the same number of Al_2O_3 units and consequently the same number of electrons.

In order to complete the electronic structure analysis of both models, the charge transfer between atoms in each model was studied with a Bader analysis [54,55]. The oxidation state of Al and O atoms were estimated by the computed Bader charges using the calculated density around each atom. For all Al atoms from both models the calculated Bader charge was exactly $+3.00$, and for O atoms it varies from -1.97 to -2.02 on both models, being the sum of the charges calculated for all 40 atoms in each model was 0.00. In spite of the noticeable little contrast between PDOS of all Al_{tet} in both models, which can be observed in Fig. 6, and was interpreted as a difference in the environment of these kinds of Al atoms, their charges are the same. In turn, the oxygen atoms in both models, as already mentioned, occupy sites with different coordination numbers namely $O_{4\text{-}fold}$ and $O_{3\text{-}fold}$ and their calculated Bader charge are consistent. The $O_{4\text{-}fold}$ charges are more negative than the $O_{3\text{-}fold}$ ones because the O^{2-} anions are easily polarized by the Al^{3+} cations [56], so the electron clouds of O^{2-} are not spherical in alumina and the Bader analysis made could describe it correctly.

5. Conclusions

The present work exposed a comparison between two γ-alumina structural models proposed in literature, a *spinel-like* and a *nonspinel* one. The study was focused on their thermodynamic stability, lattice vibrational modes, and bulk electronic properties using *ab initio* calculations. A small difference of about 4.55 kcal/mol, averaged from 0 to 1000 K, has been found in the thermodynamic stability of the two models, with the *spinel-like* model more stable. The simulated IR spectrum of the *spinel-like* model presented a profile closer to the experimental, including the assignments of the bands. These results suggest the *spinel-like* model as more adequate to describe γ-alumina, even though the electronic structure analysis shows the same features for both models, when compared with the electronic structure of the α phase, except for small differences related to the aluminum sublattice.

Acknowledgment

We thank Petrobras S/A for financial support during this work.

References

[1] J.A. Wang, X. Bokhimi, A. Morales, O. Novaro, T. López, R. Gómez, J. Phys. Chem. B 103 (1999) 299.
[2] Y. Cesteros, P. Salagre, F. Medina, J.E. Sueiras, Chem. Mater. 11 (1999) 123.
[3] S.H. Cai, S.N. Rashkeev, S.T. Pantelides, K. Sohlberg, Phys. Rev. B 67 (2003) 224104.
[4] M. Digne, P. Sautet, P. Raybaud, P. Euzen, H. Toulhoat, J. Catal. 226 (2004) 54.
[5] C. Wolverton, K.C. Hass, Phys. Rev. B 63 (2000) 024102.
[6] K. Sohlberg, S.J. Pennycook, S.T. Pantelides, Chem. Eng. Comm. 181 (2000) 107.
[7] X. Krokidis, P. Raybaud, A. Gobichon, B. Rebours, P. Euzen, H. Toulhoat, J. Phys. Chem. B 105 (2001) 5121.
[8] P. Raybaud, M. Digne, R. Iftimie, W. Wellens, P. Euzen, H. Toulhoat, J. Catal. 201 (2001) 236.
[9] H.C. Stumpf, A.S. Russel, J.W. Newsome, C.M. Tucker, Ind. Eng. Chem. 42 (1950) 1398.
[10] R. Zhou, R.L. Snyder, Acta Cryst. B 47 (1991) 617.
[11] Ľ. Smrčok, V. Langer, J. Křesťan, Acta Cryst. C62 (2006) i83.
[12] G. Paglia, C.E. Buckley, A.L. Rohl, B.A. Hunter, R.D. Hart, J.V. Hanna, L.T. Byrne, Phys. Rev. B 68 (2003) 144110.
[13] K.E. Sickafus, J.M. Wills, J. Am. Ceram. Soc. 82 (1999) 3279.
[14] P. Hohenberg, W. Kohn, Phys. Rev. B 136 (1964) 864.
[15] W. Kohn, L.J. Sham, Phys. Rev. A 140 (1965) 1133.
[16] S.S.X. Chiaro, J.L. Zotin, A.C. Faro Jr., Prep. Catal. VII 118 (1998) 633.
[17] G. Gutiérrez, A. Taga, B. Johansson, Phys. Rev. B 65 (2001) 012101.
[18] H.P. Pinto, R.M. Nieminen, S.D. Elliott, Phys. Rev. B 70 (2004) 125402.
[19] G. Paglia, A.L. Rohl, C.E. Buckley, J.D. Gale, Phys. Rev. B 71 (2005) 224115.
[20] M. Sun, A.E. Nelson, J. Adjaye, J. Phys. Chem. B 110 (2006) 2310.
[21] M. Digne, P. Raybaud, P. Sautet, B. Rebours, H. Toulhoat, J. Phys. Chem. B 110 (2006) 20719.
[22] G. Paglia, C.E. Buckley, A.L. Rohl, J. Phys. Chem. B 110 (2006) 20721.
[23] A.E. Nelson, M. Sun, J. Adjaye, J. Phys. Chem. B 110 (2006) 20724.
[24] G. Paglia, E.S. Božin, S.J.L. Billinge, Chem. Mater. 18 (2006) 3242.
[25] W.Y. Ching, L. Ouyang, P. Rulis, H. Yao, Phys. Rev. B 78 (2008) 014106.
[26] V.M. Bermudez, J. Phys. Chem. C 111 (2007) 3719.
[27] V.M. Bermudez, J. Phys. Chem. C 113 (2009) 1917.
[28] Y. Chen, C. Ouyang, S. Shi, Z. Sun, L. Song, Phys. Lett. A 373 (2009) 277.
[29] C.Y. Ouyang, Ž. Šljivančanin, A. Baldereschi, Phys. Rev. B 79 (2009) 235410.
[30] M. Digne, P. Sautet, P. Raybaud, P. Euzen, H. Toulhoat, J. Catal. 211 (2002) 1.
[31] C. Chizallet, M. Digne, C. Arrouvel, P. Raybaud, F. Delbecq, G. Costentin, M. Che, M. Sautet, H. Toulhoat, Top. Catal. 52 (2009) 1005.
[32] G. Feng, C. Huo, C. Deng, L. Huang, Y. Li, J. Wang, H. Jiao, J. Mol. Catal. A: Chem. 304 (2009) 58.
[33] E. Menéndez-Proupin, G. Gutiérrez, Phys. Rev. B 72 (2005) 035116.
[34] Y. Pan, C. Liu, Q. Ge, Langmuir 24 (2008) 12410.
[35] A.H. Reshak, S. Auluck, I.V. Kityk, Phys. Rev. B 75 (2007) 245120.
[36] A.H. Reshak, S. Auluck, I.V. Kityk, J. Solid State Chem. 181 (2008) 789.
[37] N. Ishizawa, T. Miyata, J. Minato, F. Marumo, S. Iwai, Acta Cryst. B 36 (1980) 228.
[38] A. Kirfel, K. Eichhorn, Acta Cryst. A 46 (1990) 271.
[39] P. Ballirano, R. Caminiti, J. Appl. Cryst. 34 (2001) 757.
[40] P. Giannozzi, et al. 〈http://www.quantum-espresso.org〉.
[41] J.P. Perdew, Y. Wang, Phys. Rev. B 45 (1992) 13244.
[42] D. Vanderbilt, Phys. Rev. B 41 (1990) 7892.
[43] H.J. Monkhorst, J.D. Pack, Phys. Rev. B 13 (1976) 5188.
[44] S. Baroni, P. Giannozzi, A. Testa, Phys. Rev. Lett. 58 (1987) 1861.
[45] S. Baroni, S. de Gironcoli, A. Dal Corso, P. Giannozzi, Rev. Mod. Phys. 73 (2001) 515.
[46] X. Gonze, Phys. Rev. A 52 (1995) 1096.
[47] D.A. McQuarrie, Statistical Mechanics, Harper Collins Publisher Inc., New York, 1973.
[48] J.M. Saniger, Mater. Lett. 22 (1995) 109.
[49] C. Loyola, E. Menéndez-Proupin, G. Gutiérrez, J. Mater. Sci. 45 (2010) 5094.
[50] A. Navrotsky, B.A. Whechsler, K. Geisinger, F. Seifert, J. Am. Ceram. Soc. 69 (1986) 418.
[51] J.M. McHale, A. Auroux, A.J. Perrotta, A. Navrotsky, Science 277 (1997) 788.
[52] T. Yokokawa, O.J. Kleppa, J. Phys. Chem. 68 (1964) 3246.
[53] R.H. French, J. Am. Ceram. Soc. 73 (1990) 477.
[54] G. Henkelman, A. Arnaldsson, H. Jònsson, Comput. Mater. Sci. 36 (2006) 354.
[55] W. Tang, E. Sanville, G. Henkelman, J. Phys.: Condens. Matter 21 (2009) 084204.
[56] D. Liu, Y. Jin, J. Deng, Comput. Mater. Sci. 45 (2009) 310.